Appl. Magn. Reson. 28, 343–353 (2005)

Applied Magnetic Resonance

Two-Dimensional Spectral-Spatial Image of Highly Oriented Pyrolytic Graphite

M. P. Tseitlin[1], K. M. Salikhov[1], and A. M. Ziatdinov[2]

[1] Kazan Physical-Technical Institute, Russian Academy of Sciences, Kazan, Russian Federation
[2] Institute of Chemistry, Russian Academy of Sciences, Vladivostok, Russian Federation

Received September 30, 2004; revised March 1, 2005

Abstract. Experimentally observed electron paramagnetic resonance (EPR) spectra of highly oriented pyrolytic graphite samples can be considered as a sum of three signals coming from two adjacent faces and crystal edges. Contributions from faces can be analyzed analytically by Dyson's theory based on an infinite flat conductive plate, while the contribution from edges is not described by this theory. Overlapping of these signals makes it difficult to get useful information about the sample from spectra observed. Implementation of two-dimensional spectral-spatial imaging technique proved to be helpful to solve this problem. It permits the characterization of the EPR spectrum from a selected flat spatial region located far from crystal edges where the model of the infinite flat conductive plate can be applied. By analyzing the EPR signal from spatial slices by Dyson's equation we have obtained the values of the diffusion coefficient and the surface relaxation rate.

1 Introduction

Conduction-electron spin resonance (CESR) in highly oriented pyrolytic graphite (HOPG) and its intercalation compounds is intensively studied [1–4]. The analysis of the CESR line shape gives useful information about a sample. For example, the electron spin relaxation time, the spin carrier diffusion coefficient and the surface relaxation rate can be estimated. This is usually done in the frame of Dyson's theory [5]. The ESR signal originating from spins in a conductor strongly depends on sample shape and can be analytically described only for a very limited number of object geometries (infinite plate, sphere, infinite cylinder) [6–8]. No analytic equations exist that can describe the ESR signal of a conductive object with arbitrary geometry. In the case of a sample with more complicated shape the resonance curve analysis requires numerical calculations. The problem can be solved by approximate treatment of a sample surface as a set of flat faces. It can be done if the size of a sample and the radii of surface curvature of selected regions exceed the skin depth. Some parts of the sample may not satisfy these conditions. ESR signals from each flat part of the sample

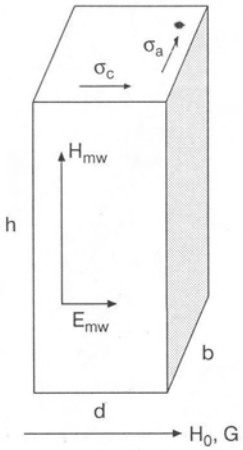

Fig. 1. Orientation of the HOPG crystal with respect to the constant external magnetic field H_0 and magnetic and electric components of the alternating field H_{mw}, E_{mw}. The direction of the constant gradient field G is parallel to H_0. The symbols h, d, and b denote height, width, and thickness of the crystal. The carbon layers of the HOPG sample are perpendicular to the plane of the paper. Conductivity along these layers σ_a exceeds the conductivity in the perpendicular direction σ_c by three orders of magnitude.

being described by Dyson's equations is summed to give a whole spectrum. This summed up spectrum may not differ much from the experimental one if most of the sample surface is represented by flat faces.

HOPG samples studied in experiments usually have the form of a parallelepiped (see Fig. 1). Microwave energy is absorbed mainly by four crystal faces parallel to the alternating magnetic field [1]. The ESR spectrum observed in the experiment can be considered as the sum of signals from lateral faces. Difficulty arises from the regions that are near to the crystal edges. Contribution of these parts of the sample to the composite spectrum cannot be described by Dyson's theory. This contribution cannot be neglected because the sample sizes are usually only a few times larger than the skin depth. Another important feature of the system under investigation is the pronounced anisotropy of conductivity and mobility of spin carriers. As a consequence, the adjacent faces of the sample give ESR signals of different shapes. In experiment one observes the sum of two signals with intensities proportional to the face squares. It is a real problem to discriminate these two signals. An approach to solve this problem is to perform EPR experiments for samples with different widths and thicknesses [1]. However, this approach cannot give unique results due to uncontrolled contribution of crystal edges to the spectrum observed. Therefore any simulation of the EPR spectrum observed as a sum of Dyson type spectra may result in incorrect values of the diffusion coefficient and of the relaxation parameters.

A very promising approach to discriminate the EPR signals from different parts of the sample, i.e., to observe the spatially selective EPR spectra, is pro-

vided by the EPR imaging technique. It allows distinguishing between signals from different parts of a sample under investigation. One can discriminate signal from the cross section of the sample at the central part where the effect of the crystal edges is expected to be minimal. The spectrum obtained in this way can be then described by a corresponding Dysonian line. Thus both problems of edge signals and overlapping of two Dysonian lines in HOPG can be solved.

In this paper we present the spectral-spatial EPR imaging of the HOPG sample. It shows how the EPR spectrum shape depends on the spatial coordinate along the gradient field. It is known from literature [9] that the mobility along carbon layers exceeds the mobility in perpendicular directions up to three orders. For our experiments, we directed the field gradient perpendicularly to carbon layers. It allowed us to avoid problems connected with spectral diffusion. At the same time, the spectra reconstructed contain information of the electron diffusion coefficient and of the surface relaxation in the direction along carbon layers. EPR imaging can be used to estimate these important physical parameters.

2 Experimental

Continuous-wave EPR measurements at room temperature were performed on an X-band spectrometer (Bruker ER 200E-SRC) with a TE_{102} cavity. The field modulation was 0.08 mT at the modulation frequency of 100 kHz. The ZZG1 gradient device was used to create a constant linear gradient of the maximum value $G_{max} = 3$ mT/mm. The sample had a thickness $d = 1.5$ mm, a width $b = 3.2$ mm and a height $h = 6.75$ mm (Fig. 1). The sample was mounted in the center of the cavity so that the magnetic component of the microwave field H_{mw} was parallel to all lateral faces of the crystal. Directions of constant magnetic field and constant gradient are shown in Fig. 1. EPR spectra, which are often called projections, were recorded at different gradient values from $-G_{max}$ to G_{max}. The spectral-spatial image is reconstructed then from a set of experimental projections.

HOPG is known to have a strong anisotropy of conductivity and electron mobility. These parameters differ in directions parallel (a) and perpendicular (c) to carbon layers. For this sample measured by four-probe method, values of conductivity were $\sigma_a = 1.2 \cdot 10^4\ \Omega^{-1}$ and $\sigma_c = 7\ \Omega^{-1}\text{cm}^{-1}$ [1], which correspond to skin layers of $\delta_a = 5 \cdot 10^{-4}$ cm and $\delta_c = 0.02$ cm at X-band.

3 Spectral-Spatial Imaging

Spectral-spatial imaging (SSI) allows reconstruction of the spin density map and the spectrum at a particular section of the sample [10–13]. The output of the SSI experiment is a pseudo-object with one spectral dimension and one, two or three spatial dimensions. In this paper we have used two-dimensional (2-D) SSI. Reconstruction of such image typically requires a set of projections recorded over

180° with an equal angular increment. Relation between the angle and the magnetic field gradient values is given by [11]

$$\tan\alpha = \frac{L}{\Delta H} G\,, \tag{1}$$

where L is the spatial length of the pseudo-object and ΔH is the spectral length of the pseudo-object. For the given values of ΔH and maximum gradient G_{max} the ratio $\tan\alpha_{max}/L$ is fixed. It is desirable to make α_{max} as large as possible. But this results in loss of spatial resolution. Compromise is achieved by using the "missing angle" algorithm. It handles an incomplete set of experimental projections and a complementary set of "missing projections" that are estimated by an iterative procedure. This procedure uses the nonnegativity constraint that the image should be positive [11]. This is valid if one works with dielectric objects and absorption spectra are registered. In the case of lossy samples, the situation changes and the image cannot be regarded as all positive.

In our experiment, we took a spectral width of the 2-D spectral-spatial image equal to $\Delta H = 2.72$ mT. This value more than four times exceeds the line width of the experimental spectrum $\Delta H_0 = 0.67$ mT, recorded in the homogeneous external magnetic field. We had to use large ΔH due to the peculiarity of Dysonian-like curves which slowly decay from central resonance part to the non-

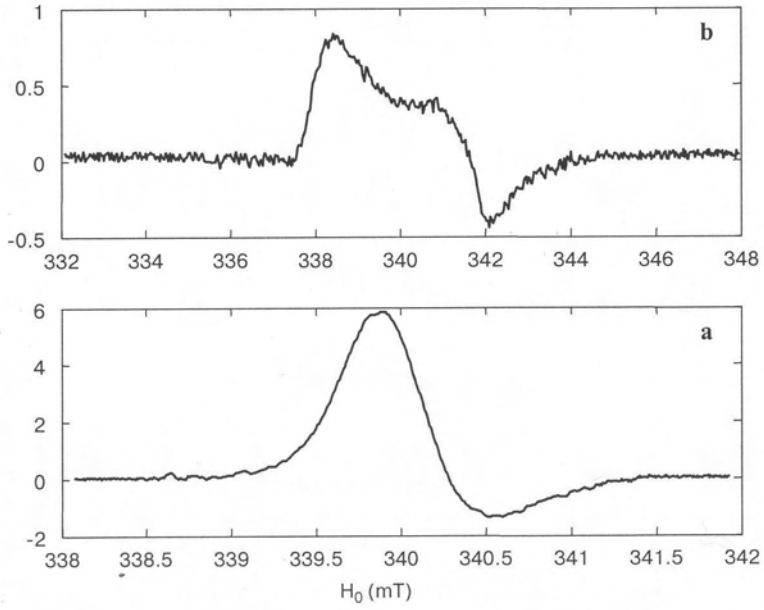

Fig. 2. Experimental spectra recorded in the homogeneous external magnetic field (**a**) and with the gradient field $G = 3$ mT/mm imposed (**b**).

resonance base line. The selected value of $\alpha_{max} = 76°$ gave us according to Eq. (1) the spatial width $L = 3.63$ mm. Thirty nine experimental projections were collected at angular increments of 4° which cover the angular region $(-\alpha_{max}, \alpha_{max})$. Six unknown "missing" projections for angles ±80, ±84 and ±88 completed the set of projections. Their values were estimated numerically. Magnetic field sweep for each spectrum was set according to the equation [11]

$$\text{sweep}(\alpha) = \frac{\sqrt{2}\Delta H}{\cos\alpha}.$$

Figure 2 shows two experimental spectra corresponding to the gradient $G = 0$ and $G = G_{max}$. The remarkable feature of these spectra is that their sign changes when the external field H_0 varies. This is a typical property of the EPR spectra for conducting and lossy-dielectric materials.

It was mentioned above that the "missing angle" algorithm cannot be used to reconstruct the sign-changing image. But nevertheless the "missing" projections can be roughly estimated by the following procedure:

1. The initial values of the missing projections are set equal to zero.
2. Experimental and zero-filled "missing" projections are used to reconstruct temporary image.
3. A new estimate of the "missing" projections is evaluated by projecting of this temporary image.

This procedure could be continued if we could impose the nonnegativity constraint. In this case, the next steps would be:

4. All projections are used to reconstruct the image.
5. All negative values in the image are replaced by zeros.
6. Steps 3–5 are repeated several times until there is no improvement in the image.

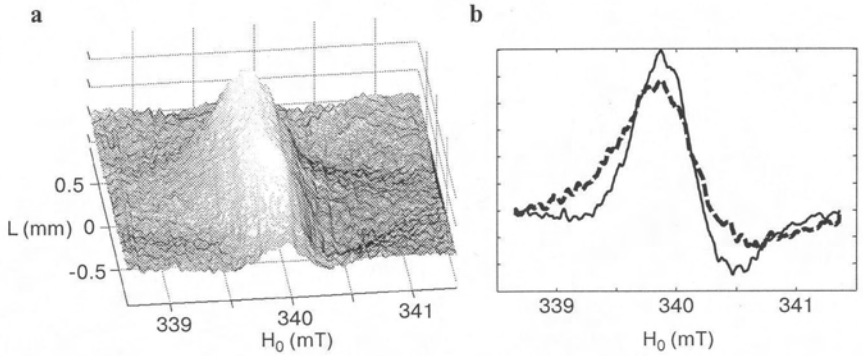

Fig. 3. 2-D spectral-spatial image of the HOPG crystal (**a**) and two EPR spectra from this image (**b**) corresponding to spatial slices $L = -0.5$ mm (solid line) and $L = 0.2$ mm (dashed line).

From three to seven iterations are usually implemented to reach the maximum available quality of the reconstructed image. But in our case we have to stop on the first iteration, since we cannot use nonnegativity constraint for conductive samples.

Now one can reconstruct the final image from the set of the experimental and estimated projections. Implementation of the approach described above gave us the 2-D image shown in Fig. 3. It represents the variation of the first derivative EPR spectrum along the spatial direction. It is seen clearly (Fig. 3b) that spectra demonstrate line shapes with positive and negative components.

It is important to note that we do not integrate experimental spectra as it is usually done in EPR imaging methods. The integral spectra obtained from conductive samples show sign-changing behavior in comparison with those detected from dielectric objects due to the admixture of the dispersion signal to the absorption signal. Dispersion curve decays to zero as $1/(\omega - \omega_0)$, where ω_0 is the resonance frequency and its derivative changes as $1/(\omega - \omega_0)^2$. That is why derivative spectra being narrower are more suitable for the imaging.

4 Results and Discussions

The Dysonian EPR line has a peculiar shape. In the central part of the spectrum its derivative has a pronounced maximum. The height of this maximum is denoted as A. One of the other characteristic features of the detected EPR signal is the minimum in the high-field part of the spectrum. The amplitude of this minimum is negative and its value is usually denoted as B. It appears [14] that the ratio A/B is a good representative parameter when analyzing the Dysonian line shape. For thick conductive plates this parameter increases from the value

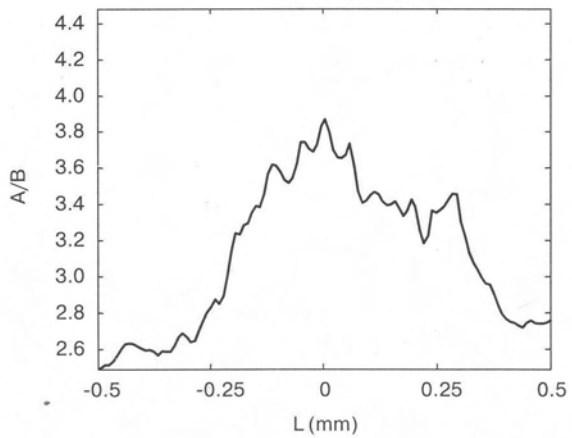

Fig. 4. Asymmetry parameter A/B of the EPR spectrum as a faction of spatial coordinate in 2-D spectral-spatial image.

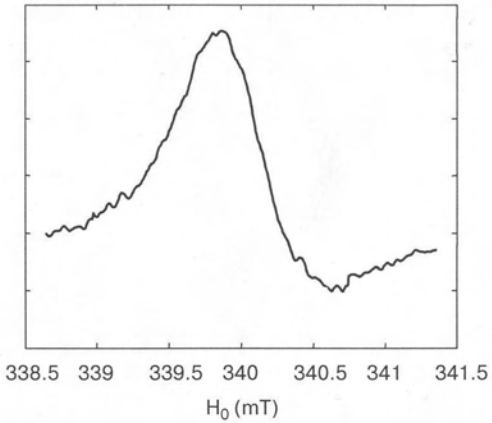

Fig. 5. EPR spectrum from the central part of the 2-D spectral-spatial image. This spectrum is expected to be undistorted by edge effects. It can be fitted by the analytical equation given by Dyson [5] to estimate the diffusion coefficient and the surface relaxation rate.

of 2.55 in the case of localized magnetic moments up to tens with increase in the diffusion coefficient and the surface relaxation rate.

Figure 4 shows the variation of the asymmetry parameter A/B along the spatial coordinate in the region of $-0.5 \leq L \leq 0.5$ which is obtained from the 2-D spectral-spatial image. It is seen that A/B reaches a maximum value in the center of the sample and decreases at the edges. As discussed above, we expect that EPR spectra in the central part of the 2-D spectral-spatial image are undistorted and can be treated by the analytical equations of the Dyson theory [5]. One of these spectra is shown in Fig. 5. We have chosen the spatial section $|L| \leq 0.25$ in the 2-D image and for this region found an average value of $A/B = 3.4 \pm 0.25$. To analyze quantitatively this value, we consider the model of an infinite conductive plate. The thickness of this plate is equal to the width of the sample under investigation, $b = 3.2$ mm. The conductivity of this plate equals σ_c so according to well-known relation

$$\delta = \frac{c}{\sqrt{2\pi\sigma\omega}}$$

the skin depth equals to $\delta = 0.2$ mm. In this case the Dysonian line shape depends on two parameters which describe spin diffusion and surface relaxation [5]

$$R = \sqrt{T_D / T_2}\,, \tag{2}$$

$$g = -\left.\frac{dM/dz}{M}\right|_{z=0}.$$

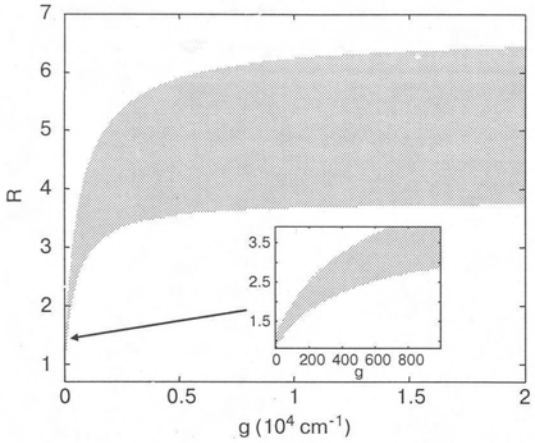

Fig. 6. Data set of R and g values compatible with the experimental asymmetry parameter $A/B = 3.4 \pm 0.25$.

Here T_D is the time that it takes for an electron to diffuse through the skin depth, i.e., $T_D = \delta_c^2/2D$, D is the spin carrier diffusion coefficient, T_2 equals the phase relaxation time of spins, M is transverse magnetization. Increasing of g and decreasing of R influence the EPR spectrum shape in a similar way, namely, increasing the ratio A/B. As a result, different sets of R and g give practically indistinguishable EPR spectra.

In order to find a region in R-g coordinates which leads to the EPR spectrum with the asymmetry parameter equal to $A/B = 3.4 \pm 0.25$, we have calculated the A/B ratio for $2 \cdot 10^5$ spectra varying the parameters R and g as $R = 0.7$ to 7 and $g = 0$ to 20000 cm^{-1}. The result is shown in Fig. 6, where $A/B = 3.4 \pm 0.25$ appears inside the black filled region. From Fig. 6 we see that a fitting of the experimental EPR spectrum might be done with the parameter R varying in the interval from 0.9 to 6.7. By calculating spectra for $g > 2 \cdot 10^4$ cm^{-1}, we could extend the black filled region infinitely. But this extension has no physical meaning. According to the equation given by Dyson [5]

$$g = \frac{3}{4}\frac{\varepsilon}{\lambda}, \tag{3}$$

where ε is the probability of spin disorientation during the collision with the surface and λ is the mean free path of the spin carriers. With ε fixed, increasing g would require decreasing λ. The efficiency of a collision of the spin carrier with the surface satisfies the condition $\varepsilon \leq 1$. Therefore, for the g values one has the condition $g < 1/\lambda$. Thus infinitely large values of g correspond to infinitely small values of the spin carriers' free path.

The diffusion coefficient is given by the Einstein law

$$D = \frac{1}{3}\lambda v\,, \tag{4}$$

where v is the mean spin carrier velocity. By substituting Eqs. (3) and (4) and taking into account Eq. (2) we can write:

$$g = K\varepsilon v R^2, \quad K = \frac{T_2}{2\delta_c^2}\,. \tag{5}$$

It is important that the parameter K in Eq. (5) can be reasonably estimated from the line width of the EPR spectrum, 0.67 mT, and the electric conductivity.

Thus, the experimental value of the ratio A/B gave the region of possible values of the parameters g and R (the black filled area in Fig. 6). At the same time the theory predicts the parabolic dependence between these two parameters given by the Eq. (5). However, the curvature of this parabola is determined by the product of ε and v which are to be found. This product being known, the range of g and R values, compatible with the experiment, would be considerably narrowed. We have taken this approach. First, we estimated K value. Relaxation time $T_2 = 10^{-8}$ s which approximately corresponds to line width ΔH_0 in homogeneous magnetic field was used in the calculations. Using the depth of the skin layer presented above, we obtain $K = 1.25 \cdot 10^{-5}$ s/cm^2. We have performed the calculations for the εv values in an interval 10 to 10^8 cm/s. For a given value of εv we have drawn the curve $g = K\varepsilon v R^2$ and have determined the values of R which are overlapping with possible values of R in Fig. 6. Figure 7 shows the possible range of R obtained as the function of v. Note, that R is practically independent of εv in the range of $10 < \varepsilon v < 10^6$, cm/s. For each given

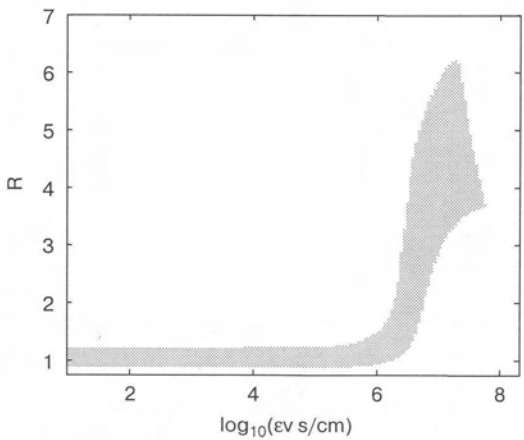

Fig. 7. Rearrangement of the data shown in Fig. 6 in the form where R is given as a function of εv.

Table 1. Minimum and maximum values of R, D, and g as a function of εv.

$\lg(\varepsilon v)$	R_{min}	R_{max}	D_{min} (10^3 cm^2/s)	D_{max} (10^3 cm^2/s)	g_{min} (cm^{-1})	g_{max} (cm^{-1})
1	0.9	1.2	14	25	+0.0	+0.0
3.8	0.9	1.2	14	25	0.1	0.1
5.3	0.9	1.3	12	25	2.0	4.2
6	1	1.5	9	20	13	28
6.3	1	2	5	20	25	100
6.5	1.2	3.8	1.4	14	56	565
7	3	5.9	0.6	2.2	1136	4167
7.2	3.3	6.2	0.5	1.8	2201	7924
7.3	3.4	6.2	0.5	1.7	2934	9976
7.6	3.7	4.4	1	1.5	6635	9953
7.8	3.7	3.7	1.5	1.5	10516	10516

value of εv the interval of R (R_{min}, R_{max}) was found. With this aim, maximum and minimum values of the diffusion coefficient and of the characteristic parameter of the surface relaxation g for the given εv can be found from calculated data represented in Fig. 7. The results obtained are shown in Table 1.

Thus, with experimental values of the ratio A/B we have obtained the possible values of D, $500 \leq D \leq 25000$ cm^2/s. Now, let us compare this result with the parameters available in literature. According to ref. 9, $v_0 = 2 \cdot 10^7$ cm/s, $\lambda_0 = 0.7 \cdot 10^{-5}$ cm. Then the diffusion coefficient is expected to be equal to $D_0 = 50$ cm^2/s. We see that this expected value of D_0 is one to two orders of magnitude less than what follows from the fitting of the experimental data. This means that either v and/or λ should have larger values. We assume that our samples are of a better quality, have a larger degree of crystallinity, therefore λ can have the larger value $\lambda \gg 10^{-5}$ cm, while for the mean velocity of the spin carriers we take $v = v_0$. In this case the possible values of λ are $7 \cdot 10^{-5}$ to $3.75 \cdot 10^{-3}$ cm. This interval might be narrowed if the efficiency ε of the spin dephasing on the surface was known. Suppose $\varepsilon = 0.1$. Then $\varepsilon v_0 = 2 \cdot 10^6$ cm/s. For this case, using the data presented in Table 1 we obtain the possible values of λ $0.75 \cdot 10^{-3} < \lambda < 3 \cdot 10^{-3}$ cm. If $\varepsilon = 0.01$, then $\varepsilon v_0 = 2 \cdot 10^5$ cm/s, and we obtain the possible values of λ $1.8 \cdot 10^{-3} < \lambda < 3.75 \cdot 10^{-3}$ cm.

Note that these estimations were done with the assumption that the relaxation time equals $T_2 = 10^{-8}$ s. We could not find any information of relaxation times of HOPG in literature, but spectra recorded at X- and Q-band had similar line widths [15]. This speaks for the homogeneous broadening and T_2 estimation from the line width is expected to be correct.

7 Conclusions

The spectral-spatial image of the HOPG crystal studied demonstrates that there is a dependence of the EPR spectrum shape on the sample boundaries. With the

SSI method we obtained an EPR spectrum that is minimally influenced by the crystal edges. Therefore, we were able to obtain the ratio A/B characterizing the intensities of the EPR signals in the central part of the spectrum. By analyzing the EPR spectrum shape one can, in principle, find the magnetic resonance parameters and spin carrier mobility parameters. However, it appears that the EPR spectrum observed and the A/B ratio obtained can be fitted by a rather broad range of those parameters. So complementary data are needed to get unique quantitative results.

Acknowledgements

This work was supported by Russian Science Support Foundation grant, RFFI grants 03-03-32602, 04-03-32135, the Russian president grant NSh-1905.2003.2 and by the CRDF grant (BRHE program).

References

1. Ziatdinov A.M., Mishchenko N.M.: Fiz. Tverd. Tela (Leningrad) **36**, 2360 (1994)
2. Ziatdinov A.M., Mishchenko N.M.: J. Phys. Chem. Solids **58**, 1167 (1997)
3. Stein R.M., Walmsley L., Rettori C.: Phys. Rev. B **32**, 4134 (1985)
4. Saint Jean M., McRae E.: Phys. Rev. B **43**, 3969 (1991)
5. Dyson F.J.: Phys. Rev. **98**, 349 (1955)
6. Webb R.H.: Phys. Rev. **158**, 225 (1967)
7. Pifer J.H., Magno R.: Phys. Rev. B **3**, 663 (1971)
8. Valiev K.: Uch. Zap. Kazan. Gos. Univ. **115**, 15 (1955)
9. Chung D.D.L.: J. Mater. Sci. **37**, 1 (2002)
10. Lauterbur P.C., Levin D.N., Marr R.B.: J. Magn. Reson. **59**, 536 (1984)
11. Maltempo M.M., Eaton S.S., Eaton G.R.: J. Magn. Reson. **72**, 449 (1987)
12. Maltempo M.M., Eaton S.S., Eaton G.R.: J. Magn. Reson. **77**, 75 (1988)
13. Eaton G.R., Eaton S.S., Ohno K.: EPR Imaging and in vivo EPR. Boca Raton, Fla: CRC Press 1991.
14. Feher G., Kip A.G.: Phys. Rev. **98**, 337 (1955)
15. Ziatdinov A.M., Kainara V.V. in: EPR in 21th Century (Kamamory A., Yamauchi J., Ohta H., eds.), pp. 236–241. Amsterdam: Elsevier 2002.